Analysis of Non- Subsampled Contourlet Transform for Medical Image Fusion

Satyanarayana, Vella
Department of ECE, JNTUCEA

P. Mohanaiah
Department of ECE, N.B.K.R Institute of Science & Technology

https://doi.org/10.5109/7183437

出版情報：Evergreen. 11 (2), pp.1286-1291, 2024-06. 九州大学グリーンテクノロジー研究教育センター
バージョン：

Analysis of Non- Subsampled Contourlet Transform for Medical Image Fusion

Vella Satyanarayana[1,*], P. Mohanaiah[2,*]
[1]Department of ECE, JNTUCEA, Anantapur, India
[2]Department of ECE, N.B.K.R Institute of Science & Technology, Vidyanagar, Nellore, A. P., India

E-mail: vellasatyanarayana414@gmail.com (V. Satyanarayana)
mohanaiah613@gmail.com (P. Mohanaiah)

(Received September 14, 2022; Revised April 8, 2024; Accepted June 14, 2024).

Abstract: In this paper, at different picture representation levels, such as the feature, pixel, decision-making, and data levels, images are presented. Pixels in pixel-level image fusion uniquely identifies a group of pixels in several source images, and the fused image may then be produced. Fused images have the advantage of being more informative than the original image and containing original data. The non-subsampled contourlet transform (NSCT) provides a multiresolution, multidirectional, and multiscale, frameworks for the calculation of discrete pictures, whereas the discrete Wavelet transform (DWT) assesses the signal's agreement with the wavelets. In this work, the energy fusion rule is applied to all DWT and NSCT frequency coefficients at the primary level. Orientation and edge strength are preserved via a fusion rule in the sub-block of the spatial field. MRI and CT scans are used as inputs for NSCT and DWT, and these images are then merged individually in the NSCT and DWT domains. The combined DWT and NSCT results are combined once over by means of spatial domain ideas. Dual-level fusion architecture is employed to maintain and improve the visual eminence of the output picture. There are both subjective and objective assessments of the performance. All NSCT and DWT frequency constants are fused using the energy fusion rule in the first phase, and then the ESOP fusion instruction is used in the second stage.

Keywords: Image, fusion, NSCT, DWT, transform, pixel.

1. Introduction

Numerous applications, including computer vision, medical imaging, military surveillance, and remote sensing, have effectively used it. This is brought on by the quick development of image sensor applications. An image that keeps all of the essential information from the source photographs and adds more details about a scenario is produced by merging images acquired with multiple sensors and from different angles [1, 2, 3]. As a result of issues such as the limits of sensors and lighting conditions, direct images cannot meet the needs of actual applications. occlusions and angles, and so on." Multiple sources of information are combined in this approach to produce an image that is both pleasing to the eye and useful to the brain[4, 5, 6, 7, 8]. It is possible to combine many photos into a single one with the use of an algorithm known as "image fusion". Fused photos provide information that is more effective and exact than the images that were used as input, and it includes all of the necessary data. It's not enough for image fusion to merely reduce data volume; the end result should be images that are simple for both humans and machines to comprehend. Image fusion is utilized in remote sensing, satellite imaging, the medical industry, and many other fields[9, 10, 11, 12, 13]. Images fused in various ways i.e., multi sensor imaging and single sensor imaging[14, 15, 16].

1.1 Single Sensor Imaging

In this system, a single sensor might not be able to gather all of the target's data. A single sensor may be used to capture images on the same modalities. Single-sensor cameras are sluggish and unable to simultaneously focus on numerous distances[17, 18, 19, 20].

1.2 Multi Sensor Imaging

Multi-sensor imaging uses two or many sensors to take the photos. Saving time is accomplished by quickly taking numerous images of the same scene[21, 22, 23]. By using a multi-sensor, for instance, many types of photos can be taken. Multiple sensors are used for more operative imaging. and produces additional data than single sensor imaging[24, 25, 26]. In this work, concepts from the first level—NSCT and DWT—as well as the second level spatial domain notions are used.

2. Methodology

The proposed structure is defined in the next section based on these perceptions.

2.1 Non-Subsampled Contour let Transform

A particular kind of multidirectional, multiscale, and multi-resolution architecture for the calculation of discrete pictures is the NSCT. The NSP has two phases: NSSP and a group of one-way filters without subsampling.

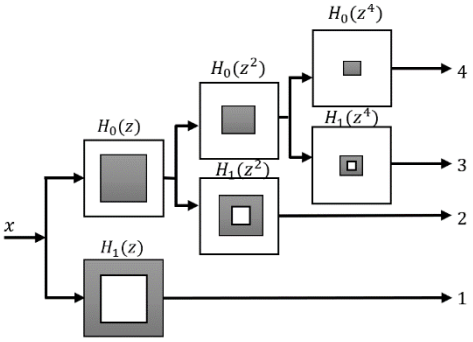

Fig. 1: Three-stage decomposition

The primary phase delivers multi-scale qualities by means of a two-channel architecture that is not sub sampled. At each stage of the NSP decomposition procedure, one HF and single LF component is produced. The NSP step that decomposes the low frequency components incrementally. N+1 subpictures are created as a result of NSP's decomposition. created using a single low-frequency image and N high-occurrence photos. Images in both their original and fragmented forms final sizes must match. An NSP decomposition with N = 3 layers is shown in Figure 1. A two-channel filter called Non sub sampled directional filter bank (NSDFB) enables directionality decomposition. if used in conjunction with fan filter banks. Each NSP scale generates 2M directional subpictures for each M level[4, 5, 7, 9, 12]. The NSDFB provides more exact information about the directionality of NSCT because it is multi-directional. These traits are fully exemplified in Figure 2.

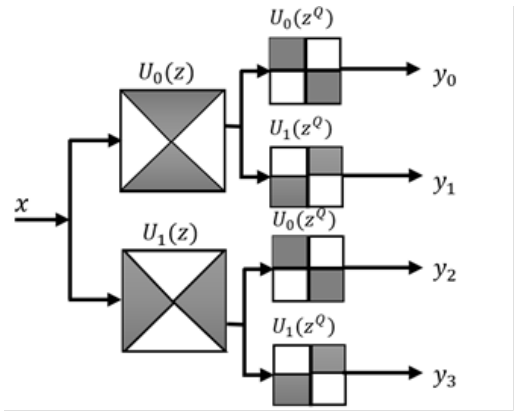

Fig. 2: 4-channel NSDFB constructed

Statistically each sub-band energy is computed using the following equation:

$$\mathrm{E1}\ (\mathrm{j,k}) = \sum_{j-1}^{j+1}\sum_{k-1}^{k+1} A\ (j,K) \quad (1)$$

$$\mathrm{E1}\ (\mathrm{j,k}) = \sum_{j-1}^{j+1}\sum_{k-1}^{k+1} B\ (j,K) \quad (2)$$

Two images, A and B, are used as examples.

2.2 Discrete Wavelet transforms (DWT)

The concept and idea behind wavelets were developed by Mallat. DWT calculates how similar two wavelets areIf the signal's form is resembles a Wavelet, then higher transform values are generated. Low transform values are obtained if the signal and wavelet are not strongly correlated. Different scales and locations are used to calculate the Transform. When processing photos, it is feasible to identify regional features by utilizing the wavelet transform as an analytical tool. A time-frequency representation of a picture is created by this transformation. The drawbacks of STFT are overcome by this transform, which also investigates non-stationary signals. Various resolutions of the signal are visible in this. Considered a mathematical microscope, this transformation The input sequence is divided into high pass and low pass sub bands by the DWT. Half of the original input samples make up each sub-band. The initial phase of DWT is input analysis, which is followed by decimation. A two-dimensional transform may be produced by combining two one-dimensional transforms. The input images are first divided by two and filtered along rows. The filtering of subpictures along columns comes next[8, 11, 13, 14, 15]. This technique divides the input into smaller band, which are discussed in Figure 3.

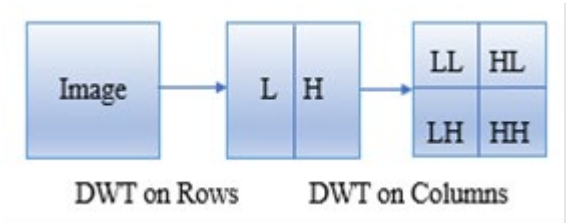

Fig. 3: Decomposition of DWT

The two-dimensional expressed using DWT

$$\psi^{\varphi}_{(j_0,u,v)} = \frac{1}{\sqrt{N \times \mathrm{N}}}\sum_{y=0}^{N-1} f\ (x,y)\phi_{(j_0,u,v)}(x,y) \quad (3)$$

$$\psi^{i}_{(j,u,v)} = \frac{1}{\sqrt{N \times \mathrm{N}}}\sum_{y=0}^{N-1} f\ (x,y)\ \psi^{i}_{(j,u,v)}(x,y) \quad (4)$$

Where $\phi_{j_{0,u,v}}(x,y) = 2^{\frac{j}{2}}\ \phi\ (2j\ x-u,\ 2j\ y-v)$ is the scaling function $\boldsymbol{\Psi^{i}_{j,u,v}} = \mathbf{2^{\frac{j}{2}}}\ \boldsymbol{\Psi^{i}}\ (2j\ x-u,\ 2j\ y-v)$ is explained purpose, $\times N$ is the size 'i' assumes row, column and diagonal values 'j' specifies scale purpose and 'u, v' standards are extending from 0,1,2…..2j $\Psi_{\varphi}(j_0,u,v)$ coefficients resemblances $f(x,y)$ and $\Psi_{\Psi}(j,u,v)$ coefficients describe detailed components of $f(x,y)$.

2.3 Spatial domain

Pixels are manipulated directly in the spatial domain. This field is not only affordable and time-effective, but also simple to learn. When comparing two edges, the edge-based similarity measure yields a comparison that is stated as

$$Q^{\frac{AB}{F}} = \frac{\sum_{j=1}^{M}\sum_{k=1}^{N}[Q_{j,k}^{AF}W_{j,k}^{X}+Q_{j,k}^{BF}w_{j,k}^{Y}}{\sum_{j=1}^{M}\sum_{k=1}^{N}[W_{j,k}^{X}+W_{j,k}^{Y}]} \quad (5)$$

The inputs and outputs are images A, B, and F, respectively. Each of the parameters is same, and they are listed below as follows:

$$Q_{j,k}^{AF} = Q_{g,j,k}^{AF} \quad (6)$$

$$Q_{j,k}^{BF} = Q_{g,j,k}^{BF}Q_{a,j,k}^{BF} \quad (7)$$

Where Q_{g}^{*F} and F Q_{α}^{*F} are ESOP standards. The usual range is from 0 to1. The fusion has a higher value than this.

3. Proposed Work and Discussions

We'll discuss some of the motivations behind our idea for merging medical pictures in this part. It is taken into account that the proposed work requires two distinct photos from the same source in order to create the composite image. Using this framework requires the registration of pixels in the source images.

3.1 Proposed dual fusion Methodology steps

Typical MRI and CT picture data are gathered and designated A and B in order to test the suggested fusion strategy. The steps in our recommended algorithm are as follows:

Step 1: Preprocessing is carried out using database-stored merged pictures. Testing frequently uses images with a resolution of 256 by 256 pixels.

Step 2: When NSCT is used on the source photos, a single LF and set of HF coefficients are produced for each level and orientation. This is known as merging at the top level. This decomposition's level(n) selections are [2, 2, 4]. There were 4,4,16 sub-bands produced at these levels. For the directional filter and the pyramidal filter, respectively, the max flat filter and the dmaxflat7 filter were used.

Step 3: To determine how much energy each coefficient possesses, apply the formula.

$$\mathrm{E1}\ (\mathrm{j},\mathrm{k}) = \sum_{j-1}^{j+1}\sum_{k-1}^{k+1} A\ (j,K) \quad (8)$$

$$\mathrm{E1}\ (\mathrm{j},\mathrm{k}) = \sum_{j-1}^{j+1}\sum_{k-1}^{k+1} B\ (j,K) \quad (9)$$

Step 4: Low-frequency fusion use low-frequency images to roughly represent the source images. The merging process uses straightforward average techniques. However, a high-quality composite image cannot be produced due to weak contrast. Therefore, we apply the Energy Fusion Rule.

$$F_j^F(\mathrm{j},\mathrm{K}) = \frac{F_j^A(j,k)}{\frac{F_j^B(j,k)}{\frac{F_i^K(j,k)}{2}}} \quad (10)$$

Step 5: High-frequency fusion: The sub-images with high-frequency and the specific elements of the source images are matched. The Each sub band's energy is computed. as follows:

$$\mathrm{F}(\mathrm{j},\mathrm{k}) = F_{l,\theta}^{A}(j,K), if\ E_{i,\theta}^{A} \geq F_{l,\mu\theta}^{B} \quad (11)$$

$$\mathrm{F}(\mathrm{j},\mathrm{k}) = F_{l,\theta}^{A}(j,K), if\ E_{i,\theta}^{A} \leq F_{l,\mu\theta}^{B} \quad (12)$$

Step 6: To create the first level fused picture F, Each and every frequency band has its inverse NSCT operation carried out on it.

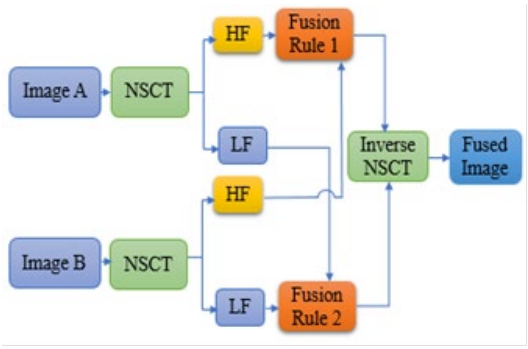

Fig. 4: NSCT fusion diagram

Step 7: For the initial degree of fusion, DWT is applied to the two source pictures. The reduced photos are 256256 pixels in size. These 256 x 256 graphics are divided into five layers: 128 x 128, 64 x 64, 32 x 32, 16 x 16, and 8 x 8. In the decomposition, Haar wavelet is used. By employing the energy fusion rule, all frequency component from both image is combined. Utilizing inverse DWT, the original picture C is recreated. Low-frequency information is linked with large portions of an image, whereas high-frequency information is connected with sharp edges and contours.

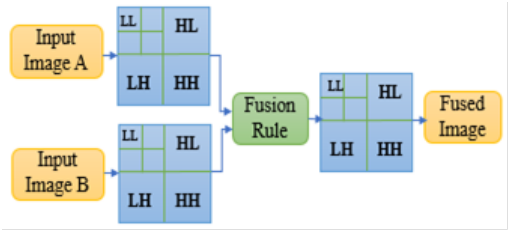

Fig. 5: DWT fusion diagram

The calculation of the energy of all sub-band make use of (1). Using the following relationship, compare the energy in each of the sub bands in both images.

Fusion of high-frequency (HF) sub-images: HF sub-images are those that include the finest details from the input images. For each strength sub band, we get:

$$C_{l,\theta}^{F}(\mathrm{j},\mathrm{k}) = C_{l,\theta}^{A}(j,K), if\ E_{i,\theta}^{A} \geq F_{l,\mu\theta}^{B} \quad (13)$$

$$C_{l,\theta}^{F}(\mathrm{j},\mathrm{k}) = C_{l,\theta}^{A}(j,K), if\ E_{i,\theta}^{A} \leq F_{l,\mu\theta}^{B} \quad (14)$$

New images should maintain their basic qualities, such as regions and outlines, by following this general approach. The sharpest changes in intensity are associated with the sub-bands with the highest energy transformation values.

Step 8: In order to create yet another fused picture, the two previously merged images, F and C, are combined once again. This is the second level fusion. Spatial technique is utilized to conduct second level fusion. The 256×256 images F and C have been broken into 32, 8×8 chunks that do not overlap one another.

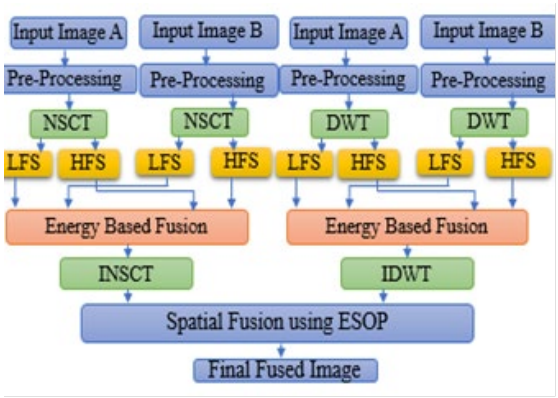

Fig. 6: Suggested System Block Diagram

Step 9: Application of edge strength and orientation preservation (ESOP) to each block is required (3)

Step 10: Choose the image block with the highest ESOP from each source image.

$$D_F(\mathrm{j},\mathrm{k}) = D_1(j,k)ESOP_1(j,k) \geq ESOP_2(j,K) \quad (15)$$

$$D_F(\mathrm{j},\mathrm{k}) = D_1(j,k)ESOP_1(j,k) \leq ESOP_2(j,K) \quad (16)$$

Blocks ESOP1 (j, k) and ESOP2 (j, k) have the greatest ESOP, respectively (j, k). It is decided that the block DF (j, k) will be the one to be used. Fuse the relevant blocks into the empty block.

Step 11: The quality of mutual information, entropy, and an edge-based similarity metric were all measured and displayed for the combined images.

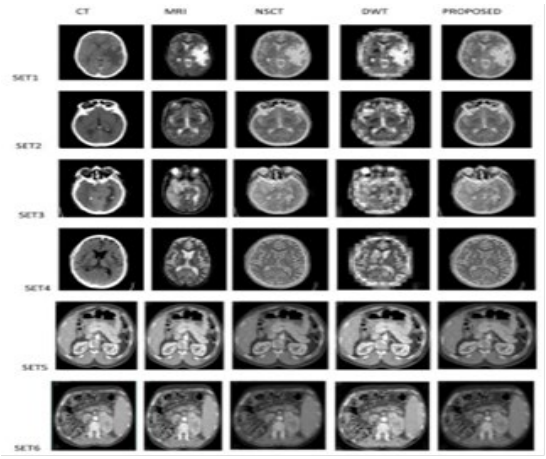

Fig. 7: The integration of many medical images

Table-1: Performance comparison of different algorithms

S. No.	Parameter	DWT	NSCT	Proposed Method
SET 1	Entropy	1.09605	2.452902	2.373987
	ESSIM	0.995904	0.997508	0.999990
	Q_{MI}	0.813503	0.688369	1.342305
SET 2	Entropy	1.001202	2.743201	4.901702
	ESSIM	0.994201	0.996999	0.99999
	Q_{MI}	0.7401	0.631718	1.318502
SET 3	Entropy	1.022605	2.755505	5.013978
	ESSIM	0.993998	0.996702	0.999909
	Q_{MI}	0.711403	0.551507	1.305605
SET 4	Entropy	1.051901	2.308404	5.098307
	ESSIM	0.994902	0.996901	0.999909
	Q_{MI}	0.736605	0.544502	1.297603
SET 5	Entropy	0.794202	1.251608	7.125209
	ESSIM	0.994801	0.998609	0.999904
	Q_{MI}	0.749902	0.619307	1.268509
SET 6	Entropy	0.584901	0.935995	7.282500
	ESSIM	0.994100	0.996900	0.999989
	Q_{MI}	0.644406	0.538900	1.257508

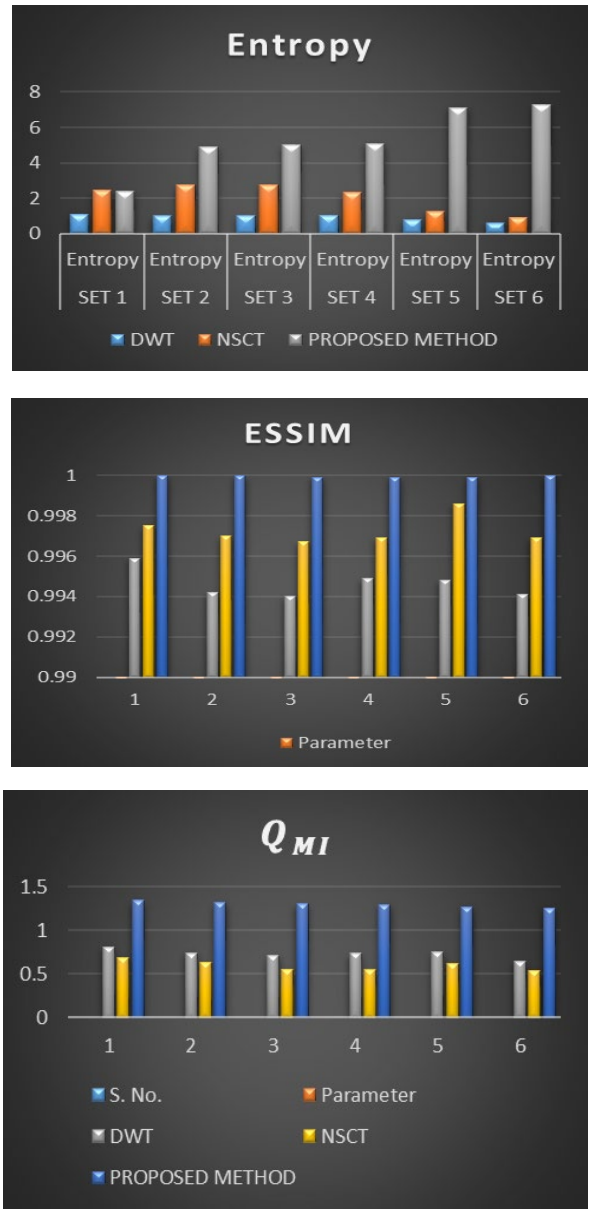

Fig. 8: Performance comparison of the fusion algorithms

4. Results and Discussions

The proposed fusion process's effectiveness is demonstrated in this section. There are certain conditions for the fusion algorithm. 1). From both of the input photos, extensive characteristics must be extracted. 2). It is not appropriate to display relics or discrepancies. 3). It must be trustworthy. They are typically evaluated both subjectively and objectively. Significant improvements are revealed by the second-level outcomes analysis of the suggested strategy. sets of images by merging two layers of information. It has been possible to increase the mutual information, entropy, edge-based similarity measure, and entropy across all. All performance metrics depend on entropy, which is beneficial During the second fusion level, for all image sets. In all cases. The similarity measure based on edges has enhanced by the second level fusion. The second level fusion has also increased the mutual information's quality when compared to DWT and NSCT.

5. Conclusion

In the proposed work, researchers are looking at medical picture fusion from many modalities since it is useful in the medical field and can lead to better diagnoses by combining high-quality images. The combined photos should, in theory, include more data than any input image, duplications and all. Two transforms are developed, and their performance metrics were evaluated. These transforms consist of a NSCT and DWT with independent first-order fusion rules and a spatial domain technique. In an experiment, the scientists used NSCT and DWT to combine two sets of merged images. Performance indicators for DWT and NSCT, respectively, include quality of mutual information, edge-based similarity measure and entropy. Instead, it has been demonstrated that the dual level fusion method produces good outcomes.

References

1) Ellmauthaler, A., Pagliari, C.L. and Da Silva, E.A., "Multiscale image fusion using the undecimated wavelet transform with spectral factorization and nonorthogonal filter banks." *IEEE Transactions on image processing*, *22* (3) 1005-1017 (2012). https://doi.org/10.1109/TIP.2012.2226045
2) Li, S. and Yang, B., "Hybrid multiresolution method for multisensor multimodal image fusion." *IEEE Sensors Journal*, *10* (9) 1519-1526 (2010). https://doi.org/10.1109/JSEN.2010.2041924
3) Nair, T.G. and Sharma, R., "Accurate merging of images for predictive analysis using combined image." In *2013 International Conference on Signal Processing, Image Processing & Pattern Recognition*, 169-173 (2013). https://doi.org/10.1109/ICSIPR.2013.6497980
4) Cao, L., Jin, L., Tao, H., Li, G., Zhuang, Z. and Zhang, Y., "Multi-focus image fusion based on spatial frequency in discrete cosine transform domain." *IEEE signal processing letters*, *22* (2) 220-224 (2014). https://doi.org/10.1109/ LSP.2014. 2354 534
5) Li, S. and Yang, B., "Multifocus image fusion by combining curvelet and wavelet transform." *Pattern recognition letters*, *29* (9) 1295-1301 (2008). https://doi.org/10.1016/j.patrec.2008.02.002
6) Srivastava, R., Prakash, O. and Khare, A., "Local energy-based multimodal medical image fusion in curvelet domain." *IET computer vision*, *10* (6) 513-527 (2016). https://doi.org/10.1049/iet-cvi.2015.0251
7) Yang, S., Wang, M., Jiao, L., Wu, R. and Wang, Z., "Image fusion based on a new contourlet packet." *Information Fusion*, *11* (2) 78-84 (2010). https://doi.org/10.1016/j.inffus.2009.05.001
8) Bhateja, V., Patel, H., Krishn, A., Sahu, A. and Lay-

Ekuakille, A., "Multimodal medical image sensor fusion framework using cascade of wavelet and contourlet transform domains." *IEEE Sensors Journal*, *15* (12) 6783-6790 (2015). https://doi.org/10.1109/JSEN.2015.2465935

9) Pal, A., "Estimating the Coverage Performance of a Wireless Sensor Network Considering Boundary Effects in the Presence of Sensor Failure." *EVERGREEN Joint Journal of Novel Carbon Resource Sciences & Green Asia Strategy*, 8 (3) 601-609 (2021). https://doi.org/10.5109/4491652
10) Choudhary, S., Sharma, A., Gupta, S., Purohit, H. and Sachan, S., "Use of RSM technology for the optimization of received signal strength for LTE signals under the influence of varying atmospheric conditions." *EVERGREEN Joint Journal of Novel Carbon Resource Sciences & Green Asia Strategy*, 7 (4) 500-509 (2020). https://doi.org/10.5109/41 50469
11) Kong, W. and Lei, Y., "Technique for image fusion between gray-scale visual light and infrared images based on NSST and improved RF." *Optik*, *124* (23) 6423-6431 (2013). https://doi.org/10.1016/j.ijleo. 2013.05.038
12) Nandan, D., Singh, M.K., Kumar, S. and Yadav, H.K., 2022. Speaker Identification Based on Physical Variation of Speech Signal. *Traitement du Signal*, *39*(2) 711-716 (2022). https://doi.org/10.18 280/ts.390235
13) Arthur, L., Cunha, D., Zhou, J. and Do, M.N., "The nonsubsampled contourlet transform: theory, design, and applications." *IEEE Trans. Image Process*, *15* (10) 3089-3101 (2006). https://doi.org/10.1109/TIP. 2006.877507
14) Ben-Shoshan, Y. and Yitzhaky, Y., "Improvements of image fusion methods." *Journal of Electronic Imaging*, *23* (2) 023021 (2014). https://doi.org/10. 1117/1.JEI.23.2.023021
15) Wang, N., Ma, Y. and Wang, W., "DWT-Based Multisource Image Fusion Using Spatial Frequency and Simplified Pulse Coupled Neural Network." *Journal of Multimedia*, *9* (1) 159-165 (2014). http://dx.doi.org/10.4304/jmm.9.1.159-165
16) Meher, B., Agrawal, S., Panda, R. and Abraham, A., "A survey on region-based image fusion methods." *Information Fusion*, *48*, 119-132 (2019). https://doi.org/10.1016/j.inffus.2018.07.010
17) Choudhary, S., Sharma, A., Srivastava, K., Purohit, H. and Vats, M., "Read range optimization of low frequency RFID system in hostile environmental conditions by using RSM approach." *EVERGREEN Joint J. Novel Carbon Resour. Sci. Green Asia Strategy*, *7* (03) 396-403 (2020). https://doi.org/10.5109/4068619
18) Narindrasani, S. and Fuad, H., "The Role of Captivation and Sensation in Pleasurable Experience to Enhance Wayfinding Process." *EVERGREEN Joint Journal of Novel Carbon Resource Sciences & Green Asia Strategy*, 7 (1), 67-71 (2020). https://doi.org/10.5109/2740948
19) Liu, R., Liu, J., Jiang, Z., Fan, X. and Luo, Z., "A bilevel integrated model with data-driven layer ensemble for multi-modality image fusion." *IEEE Transactions on Image Processing*, *30*, 1261-1274 (2020). https://doi.org/10.1109/TIP.2020.3043125
20) Mouli, D.C., Kumar, G.V., Kiran, S.V. and Kumar, S., "Video Retrieval Queries of Large Scale Images: An Efficient Approach." In *2021 6th International Conference on Signal Processing, Computing and Control (ISPCC)*, 247-250 (2021). https://doi.org/ 10.1109/ISPCC53510.2021.9609382
21) Tan, W., Thitøn, W., Xiang, P. and Zhou, H., "Multi-modal brain image fusion based on multi-level edge-preserving filtering." *Biomedical Signal Processing and Control*, *64*, 102280 (2021). https://doi.org/10. 1016/j.bspc.2020.102280
22) Diwakar, M., Tripathi, A., Joshi, K., Sharma, A., Singh, P. and Memoria, M., "A comparative review: Medical image fusion using SWT and DWT." *Materials Today: Proceedings*, *37*, 3411-3416 (2021). https://doi.org/10.1016/j.matpr. 2020.09.278
23) Xiao, B., Ou, G., Tang, H., Bi, X. and Li, W., "Multi-focus image fusion by hessian matrix-based decomposition." *IEEE Transactions on Multimedia*, *22* (2) 285-297 (2019).https://doi.org/ 10.1109/TMM.2019.2928516
24) Fauzan, A., Ega, H.M., Sigalingging, J.A. and Nugroho, Y.S., "Analysis of Heat Gains from Flat Plate Heater Measured using Multi-Axis Heat Flux Sensors." *EVERGREEN Joint Journal of Novel Carbon Resource Sciences & Green Asia Strategy*, 8 (4) 844-849 (2021). https://doi.org/10.5109/47 42130
25) Shaiden, A.S., Islam, S. and Subramaniam, K., "Android based Digital Steganography Application using LSB and PSNR Algorithm in Mobile Environment." *EVERGREEN Joint Journal of Novel Carbon Resource Sciences & Green Asia Strategy*, 8 (2) 421-427 (2021). https://doi.org/10.5109/44 80724
26) Weake, N., Pant, M., Sheoran, A., Haleem, A. and Kumar, H., "Optimising parameters of fused filament fabrication process to achieve optimum tensile strength using artificial neural network." *EVERGREEN Joint Journal of Novel Carbon Resource Sciences & Green Asia Strategy*, *7* (3) 373-381 (2020). https://doi.org/10.5109/40 68614